

LA-UR-05-2597

Approved for public release;
distribution is unlimited.

Title: UNCERTAINTY ANALYSIS, MODEL ERROR, AND ORDER
SELECTION FOR SERIES-EXPANDED, RESIDUAL
STRESS INVERSE SOLUTIONS

Author(s): Michael B. Prime (ESA-WR)
Michael R. Hill (U.C. Davis)

Submitted to: Journal of Engineering Materials and Technology
2006, Volume 128, Number 2, pp. 175-185.



Los Alamos National Laboratory, an affirmative action/equal opportunity employer, is operated by the University of California for the U.S. Department of Energy under contract W-7405-ENG-36. By acceptance of this article, the publisher recognizes that the U.S. Government retains a nonexclusive, royalty-free license to publish or reproduce the published form of this contribution, or to allow others to do so, for U.S. Government purposes. Los Alamos National Laboratory requests that the publisher identify this article as work performed under the auspices of the U.S. Department of Energy. Los Alamos National Laboratory strongly supports academic freedom and a researcher's right to publish; as an institution, however, the Laboratory does not endorse the viewpoint of a publication or guarantee its technical correctness.

Uncertainty, Model Error, and Order Selection for Series-Expanded, Residual-Stress Inverse Solutions

Michael B. Prime
Engineering Sciences and Applications Division
Los Alamos National Laboratory
Los Alamos, NM 87545 USA
prime@lanl.gov
voice: +1-505-667-1051
fax: +1-505-665-6333

Michael R. Hill
Mechanical and Aeronautical Engineering Department
University of California
Davis, CA, 95616 USA

Abstract

Measuring the spatial variation of residual stresses often requires the solution of an elastic inverse problem such as a Volterra equation. Using a maximum likelihood estimate (least squares fit), a series expansion for the spatial distribution of stress or underlying eigenstrain can be an effective solution. Measurement techniques that use a series expansion inverse include incremental slitting (crack compliance), incremental hole drilling, a modified Sach's method, and others. This paper presents a comprehensive uncertainty analysis and order selection methodology, with detailed development for the slitting method. For the uncertainties in the calculated stresses caused by errors in the measured data, an analytical formulation is presented which includes the usually ignored but important contribution of covariances between the fit parameters. Using Monte Carlo numerical simulations, it is additionally demonstrated that accurate uncertainty estimates require the estimation of model error, the ability of the chosen series expansion to fit the actual stress variation. An original method for estimating model error for a series expansion inverse solution is presented. Finally, it is demonstrated that an optimal order for the series expansion can usually be chosen by minimizing the estimated uncertainty in the calculated stresses.

Terminology

Variable	Matrix Size	Definition
a_i	$m \times 1$	Slit depth i
A_j	$n \times 1$	Coefficient for j th term in series expansion of stresses
$[B]$	$n \times m$	Matrix that multiplies measured strains to determine $\{A\}$
$C_j(a_i)$	$m \times n$	Calibration coefficient at $a = a_i$ for P_j
e_i	$m \times 1$	Actual error in calculated stress at $x = a_i$
i		Index for number of slit depths, $i = 1, m$
j		Index for terms in series expansion, $j = 1, n$
m		Number of slit depths
n		Number of terms in series expansion
$P_j(x_i)$	$m \times n$	j th term of series expansion evaluated at $x_i = a_i$
$s_{model,i}$	$m \times 1$	Uncertainty in stress at $x = a_i$ due to model error
$s_{\varepsilon,i}$	$m \times 1$	Uncertainty in stress at $x = a_i$ from strain measurement error
$s_{total,i}$	$m \times 1$	Total uncertainty in stress at $x = a_i$
t		Thickness of specimen at cut location
$u_{\varepsilon,i}$	$m \times 1$	Uncertainty in strain measured when $a = a_i$
V	$n \times n$	Matrix of covariances $u_{A_k A_l}^2$
x		Direction of slit depth
y		Direction normal to slit plane
ε_i	$m \times 1$	Measured strain when $a = a_i$
$\varepsilon_{f,i}$	$m \times 1$	Fitted strain for $a = a_i$
$\varepsilon_{r,i}$	$m \times 1$	Randomized strain (random noise added) for $a = a_i$
σ_i	$m \times 1$	Residual stress σ_y determined for $x = a_i$
$\bar{\sigma}_i$	$m \times 1$	Residual stress at $x = a_i$ averaged over solution orders $n = a$ to b
$[\]^T, \{ \}^T$		The transpose of a matrix or a column-vector
$\bar{e}, \bar{s}, \bar{u}$		Root-mean-square (rms) average of vector entries

1. Introduction

Many methods for measuring residual stress require the solution of an elastic inverse problem in order to determine the stresses from the measured data. An increasingly popular method for solving the inverse problem is to express the spatial variation of residual stresses as a series expansion in some convenient set of basis functions. By using a least squares fit to determine the coefficients in the series expansion, the method is quite tolerant of noise in the experimental data and can provide good spatial resolution of stresses. Although briefly mentioned for application with

the Sach's method [1], the series expansion approach was first applied to residual stress measurement for the incremental hole drilling method using a power series expansion [2] and also for a sectioning method for measuring through-thickness stresses in pipe using Legendre polynomials [3]. Series expansion was soon adopted for use with the crack compliance method [4,5], now known as incremental slitting, where it has been used extensively. Series expansion has also been used with the ring core method [6], to extend Sachs' boring out method to non-axisymmetric stresses [7,8], with various other measurements [9,10], and to determine residual stress via an underlying spatial distribution of eigenstrain [11-17].

First, the present study extends previous formulations for uncertainty analysis in series expanded inverse solutions for residual stresses. Estimates of uncertainties caused by measurement errors previously ignored the covariances between the fit parameters. These covariant terms are crucial for accurate uncertainty estimation with least squares fits, and their effects are included in this work. Also, the formulation is extended to include the individual uncertainty in each measured data point, which can also be important.

Second, this work addresses a major shortcoming in previous uncertainty estimates, which then allows for an objective selection of an optimal number of terms for a given set of experimental data. A study of uncertainty for hole drilling measurements pointed out that actual stresses, when they could not be represented by the chosen series expansion, could lie outside of the calculated probability bounds [18]. Such errors can be termed "model error," and a method for estimating model error is presented in this work. Only with an accurate estimate of model error will the choice of optimal expansion order based on minimizing the stress uncertainty [19] give the actual optimal solution. Without model error, a conventional uncertainty estimate is generally non-conservative, sometimes by more than an order of magnitude.

2. Uncertainty Analysis

Several residual stress measurement methods based on incremental material removal share a common mathematical formulation for the elastic inverse problem. These methods include slitting, hole drilling, ring core, layer removal and axisymmetric Sachs' boring out. Three of these methods are illustrated in Figure 1. Since series expansion is most commonly used with the slitting method, this work presents the equations based on slitting notation.

2.1. Slitting Equations

In the slitting method, a narrow slit is incrementally cut into a part containing residual stresses. Stresses are relaxed and the part deforms, which is assumed to occur elastically. At an appropriate location strains are measured at discrete slit depths, a ,

$$\varepsilon(a_i) = \varepsilon_i \quad (1)$$

where there are m slit depths $i = 1, m$. Assuming that the stresses do not vary in the z -direction, the strain measured at an arbitrary cut depth is related to the residual stresses that originally existed on the plane of the cut by a Volterra equation of the first kind

$$\varepsilon(a) = \int_0^a c(a, x) \sigma_y(x) dx, \quad (2)$$

where c is a function of the geometry and the material's elastic constants. Since a closed-form inverse solution for $\sigma_y(x)$ is not available, it is assumed that the stress can be approximated as an expansion of analytic basis functions, $P_j(x)$

$$\sigma_y(x_i) = \sigma_i = \sum_{j=1}^n A_j P_j(x_i) = [P] \{A\}. \quad (3)$$

The second equality introduces matrix notation for convenience; $[P]$ has rows corresponding to spatial positions x_i and columns corresponding to terms j in the series expansion. The stress is defined for any x value in the domain, but it is convenient to evaluate stresses and uncertainties at

the x values corresponding to the slit depths, $x_i = a_i$. The solution for σ now requires choosing an expansion order n and determining the basis function amplitudes A_j . The solution strategy requires determining the strain release $C_j(a_i)$ that would occur at $a = a_i$ if $\sigma_y(x)$ were exactly given by $P_j(x)$. Using elastic superposition, the strain that would be measured for the $\sigma_y(x)$ from Eq. 3 is then given by

$$\varepsilon_f(a_i) = \varepsilon_{f,i} = \sum_{j=1}^n A_j C_j(a_i) = [C]\{A\} \quad (4)$$

where the subscript f refers to these calculated strains being determined by a least squares fit minimizing the difference between the measured strains, ε , and calculated strains

$$\{A\} = \left[([C]^T [C])^{-1} [C]^T \right] \{\varepsilon\} = [B]\{\varepsilon\}. \quad (5)$$

Using the notation $[B]$ allows the derivations later in this paper to be applied for various modifications to the maximum likelihood estimate (least squares fit) such as a weighted fit or even to a Bayesian estimate like Tikhonov regularization. See the Appendix for the form $[B]$ takes for such cases.

2.2. Major Sources of Uncertainty

Only the two main error sources are considered in this work. In most practical cases, these two sources make the most significant contributions to stress uncertainty. This paper will later demonstrate that model error is one of these two main error sources and give the first procedure for calculating model error. The other main error source for series expanded residual stresses is errors in the measured data, strains in this case. Strain errors have long been recognized as a main error source, and this assumption was confirmed by a more detailed study [18]. The calculation of stress uncertainty caused by random strain errors is reexamined in this work to provide a simple and

accurate analytical formulation. A previous analytical approximation [18] did not include covariances, which makes the approximation increasingly inaccurate as the expansion order increases. Previous accurate analyses [19-21] used a numerically intensive Monte Carlo procedure, which is not necessary. Systematic errors in the strain data, such as a zero-shift, are less likely and also have been previously studied and shown to cause fairly small errors in the calculated stresses [22,23].

Other significant errors are possible and should be minimized through careful experimental procedure. Many other likely error sources can be grouped together as geometric errors. They include errors in assumed hole or slit depth, gage location and orientation, hole eccentricity, and the shape of the hole or slit compared to the assumptions used to calculate calibration coefficients (e.g., $[C]$ in Eq. 4). These errors can be effectively eliminated by measuring such geometric quantities after the experiment and then calculating $[C]$ for the actual geometry [24]. When such calculations are not possible, these errors can be significant and should be accounted for [25]. Other likely error sources include violations of the assumptions used to calculate the stresses. For example, plasticity during stress relaxation violates the elasticity assumption. Such plasticity can be a major source of errors in hole drilling measurements [26]. Another major assumption is that the method used to introduce the hole or slit does not induce stresses. Careful machining can generally limit such errors [27,28]. In some cases with high quality data, the strain error and model error can be so low that these other errors are significant and should be included if realistic error bounds are desired.

2.3. Propagated Uncertainty

Before specifically considering random strain errors, the general error propagation formulation for series expanded stresses is presented. The derivation generally follows the notation and terminology of Bevington and Robinson [29]. The uncertainty in the calculated stress at each depth is determined from a first order expansion of the propagated uncertainty in the fit coefficients:

$$s_i^2 = u_{A_1}^2 \left(\frac{\partial \sigma_i}{\partial A_1} \right)^2 + u_{A_2}^2 \left(\frac{\partial \sigma_i}{\partial A_2} \right)^2 + \dots + 2u_{A_1 A_2}^2 \left(\frac{\partial \sigma_i}{\partial A_1} \right) \left(\frac{\partial \sigma_i}{\partial A_2} \right) + \dots \quad (6)$$

where generally u_h is used for uncertainty in a parameter h , but s instead is used for uncertainty in stress in order to simplify notation later on. The covariant terms, $u_{A_k A_l}^2$ with $k \neq l$, make important contributions to the uncertainties in parameters determined by least-squares fitting [29], so they cannot be taken as zero here as they often are in other situations. From Eq. (3)

$$\frac{\partial \sigma_i}{\partial A_j} = P_j(x_i). \quad (7)$$

Substituting into Eq (6), using symmetry in the covariant terms, and writing in matrix form gives

$$\{s_i^2\} = \text{diag}([P][V][P]^T) \quad (8)$$

where V is the matrix of covariances $u_{A_k A_l}^2$ and *diag* indicates forming a vector from the matrix elements on the diagonal. Individual s_i are obtained by taking the square root of vector elements.

2.3.1. Random Errors in Strain Data

For the major source of experimental uncertainty, the measured strains, the matrix of the covariances of the A_i is calculated considering the uncertainty in the measured strains

$$V_{kl} = u_{A_k A_l}^2 = \sum_{i=1}^m \left[u_{\varepsilon,i}^2 \frac{\partial A_k}{\partial \varepsilon_i} \frac{\partial A_l}{\partial \varepsilon_i} \right]. \quad (9)$$

where $u_{\varepsilon,i}$ is the uncertainty in the strain measured when $a = a_i$. From differentiating Eq (5) one gets

$$\frac{\partial A_k}{\partial \varepsilon_i} = B_{ki}. \quad (10)$$

Substituting into Eq (9) and writing in matrix form gives

$$[V] = [B][\text{DIAG}\{u_{\varepsilon}^2\}][B]^T \quad (11)$$

where *DIAG* indicates a diagonal matrix whose diagonal elements are the elements of the vector.

Eq. 11 can now be substituted back into Eq (8) to get the vector of stress uncertainties

$$\{s_{\varepsilon,i}^2\} = \text{diag}([P][B][\text{DIAG}\{u_{\varepsilon}^2\}][B]^T [P]^T) \quad (12)$$

where the additional subscript ε on s indicates that the source of this stress uncertainty is the uncertainty in the measured strains. To avoid confusion with the uncertainty in the strains themselves, $u_{\varepsilon,i}$, this uncertainty in stress will be referred as “measurement” uncertainty.

2.3.2. Estimating Uncertainty in Individual Strains

To achieve the best possible estimates of stress uncertainty over a wide range of situations without relying on *a priori* estimates, a somewhat unconventional approach is used to supplement the estimate of the uncertainty in the measured strains to be used in Eq 12. The inherent experimental uncertainty should be the primary estimate of the strain uncertainty. However, the strain misfit, the difference between the measured strains and those calculated by the least squares fit, are used if they exceed the estimated inherent uncertainty. The assumption is that using a strain uncertainty lower than the misfit would underestimate the resulting stress uncertainty. An estimate of the standard deviation of the strain misfit, unbiased by the number of degrees of freedom in the series expansion, is given by

$$\bar{u}_{\varepsilon} = \sqrt{\frac{1}{m-n} \sum_{i=1}^m (\varepsilon_i - \varepsilon_{f,i})^2} \quad (13)$$

where the overbar indicates a root-mean-square (rms) average over all measured strains. To be consistent with this average, the uncertainty of an individual value can be taken as

$$u_{\varepsilon,i} = \sqrt{\frac{m}{m-n}} |\varepsilon_i - \varepsilon_{f,i}|. \quad (14)$$

2.4. Model Error/Uncertainty

In the general case when actual stresses cannot be perfectly fit by the chosen series expansion, a conventional analysis of all the propagated uncertainties fails to adequately estimate total uncertainty [18]. The propagated uncertainty analysis implicitly assumes that the “model,” the series expansion, can match the actual stress. When it cannot match, the uncertainty is underestimated as will be demonstrated. This type of error is commonly referred to as model error. To be consistent with the rest of this paper, the analytical estimate of the model error will be referred to as model uncertainty. For too low an expansion order, one that does not adequately fit the data, the model uncertainty should represent that increasing the expansion order will better capture the stress profile. For expansion orders in the neighborhood of some optimal fit, the model uncertainty should reproduce the observation that the fit can be relatively stable in this region.

First it must be assumed that the chosen basis functions span the space of physically possible stress profiles. Such a series could in principle reproduce the actual stresses. One can then argue that the series truncation results in the error. Therefore, the expansion order, n , is treated as a parameter with inherent uncertainty. Analogous to Eq. 6, the stress uncertainty from uncertainty in n is

$$s_{model,i}^2 = u_n^2 \left(\frac{\partial \sigma_i}{\partial n} \right)^2 \quad (15)$$

where there are no covariant terms since n is a single parameter. Because n must be integer, analytical evaluation of this expression is not possible. A finite difference could be used to estimate the partial derivative, but that leaves the value of u_n still somewhat problematic since n is not experimentally measured, and it is hard to estimate its uncertainty. Therefore an approach based loosely on Monte Carlo analysis is employed. Unlike in conventional Monte Carlo analysis, there is not a random distribution of n to draw from. Therefore stresses for different values of n are

calculated. At each depth where stress is calculated, x_i , we take a standard deviation of the stresses calculated for different order expansions

$$s_{model,i}^2(n) \approx \frac{1}{N-1} \sum_{k=a}^b (\sigma_i(n=k) - \bar{\sigma}_i)^2 \quad (16)$$

where the average stress at $x = a_i$, $\bar{\sigma}_i$, is averaged over the expansion orders from $a \leq n \leq b$ but not averaged over other depths. N is the number of stress solutions in the sum, $b - a + 1$. The calculation is repeated at each cut depth.

Two conflicting goals affect the choice of a and b . On one hand, the estimate should span a large range in order to draw a large number of samples from the population to get a converged estimate. For example, a two-term estimate with $b = a + 1$ could give a false estimate of zero model uncertainty if the data happened to be orthogonal to one term in the series. On the other hand, the estimate should span as small a range as possible in order to resolve the change in model error as a function of n .

A three-term model uncertainty works well for relatively high order expansions, like for through-thickness, slitting measurements where generally 4-11 terms in the expansion are sufficient and reasonable. Using $a = n - 1$ and $b = n + 1$ provides a reasonable compromise between small and large n -ranges. A two-term model error is the best compromise for lower order expansions such as a power-series expansion of hole drilling stresses where n is usually limited to only 1 or 2 [30]. Because of ill-conditioning of the hole-drilling results with increasing order, taking $a = n$ and $b = n + 1$ helps prevent the selection of a too-high-order solution.

2.5. Total Uncertainty

The total uncertainty is obtained by pointwise combining the individual uncertainties in quadrature since they are assumed to be independent

$$S_{total,i} = \sqrt{S_{\varepsilon,i}^2 + S_{model,i}^2} \quad (17)$$

from which an average uncertainty \bar{s}_{total} can be calculated using an rms average over the cut depths. Because the errors tend to come from many independent small effects, we assume a normal distribution. Therefore, there should be a 68% probability that the actual errors are contained within the one standard deviation uncertainties used in this paper. Multiplying by 1.64 to get 90% probability bounds may be wise in practice [18].

2.6. Discontinuous Stress Profiles

All of the measurement and model uncertainty calculations described above will work for discontinuous stress profiles if appropriate basis functions are used. Discontinuous stress profiles are most commonly encountered in layered parts. The discontinuity can be handled by using separate series expansions in each layer [31,32]. With such an approach, the stress results are somewhat unstable near the discontinuity, which will be correctly reflected in larger uncertainty estimates. A more stable solution for the stress discontinuity can be achieved using a continuous series expansion for the underlying inherent strains [33]. Again, the approach in this paper will give appropriate uncertainty estimates. However, in the case where the stress profile is discontinuous and continuous functions are used, the uncertainty estimate will be insufficient.

3. Numerical Methods and Simulation

A numerical simulation was used to examine the uncertainty analysis because the sources of error could be isolated, and the uncertainty estimate could be compared to actual errors. It was desired to examine the behavior of the uncertainty estimate over a wide range of orders. Therefore, a through-thickness slitting experiment was chosen for the simulation because it allows the use of higher order expansions than hole drilling. A beam with thickness of $t = 1$ was simulated and the

beam was $10t$ long. A zero-width slit was considered at the exact mid-length of the beam. The slit was extended in increments of $da = 0.02t$ to a final depth of $a = 0.98t$ giving $m = 49$ depths. The strains were calculated for a strain gage with length $0.01t$ centered directly opposite the slit. Since 2D solutions under applied loads and free of body forces are independent of elastic constants, the material behavior was conveniently taken as elastic with an elastic modulus of 1 and Poisson's ratio of zero.

For the series expansion inverse, the standard choice was made for the basis functions. Legendre polynomials are used for through-thickness stresses because omitting the uniform and linear polynomials enforces equilibrium. Thus the expansion in Eq. 3 starts with the 2nd order Legendre polynomial, $P_1(x) = L_2(x)$.

$$\sigma_i = \sum_{j=1}^n A_j L_{j+1}(x_i) \quad (18)$$

The domain for the polynomials is the full thickness of the beam. Near-surface measurements, where equilibrium should not be enforced, often use other basis functions.

3.1. Stress Profiles

Residual-stress profiles were chosen to allow examination of model uncertainty and measurement uncertainty both in isolation and in combination. Of the many such stress profiles examined during this study, the two reported here, shown in Figure 2, demonstrate both the strength and limitations of the uncertainty estimates and order selection process. They are similar profiles that might be produced by introducing compressive stresses on one surface of a beam to a depth about 25% of the thickness. The rest of each profile is mostly what one would expect by the re-establishment of equilibrium after the introduction of compressive stresses. The first stress profile was a polynomial distribution so it could be fit exactly by the series expansion. The second stress profile came from the Gaussian function so that it could not be fit exactly by polynomials and could

therefore be expected to have significant model error. A linear term was added to the Gaussian function to establish force and moment equilibrium. Both stress profiles were normalized to give a peak compressive stress of negative one. The polynomial distribution is given by

$$\begin{aligned}\sigma(x) &= 0.0466845(-24L_2(x) + 10L_3(x) + 8L_4(x) - 5L_5(x)) \\ &= 0.0466845(-1260x^5 + 3710x^4 - 3720x^3 + 1326x^2 - 46x - 21)\end{aligned}\quad (19)$$

And the Gaussian distribution is given by

$$\sigma(x) = 2.28735 \left(0.609825 - 0.857365x - e^{-\left(\frac{x-0.05}{0.15}\right)^2} \right). \quad (20)$$

3.2. Finite Element simulation

By using the same finite element model to simulate the slitting experiment and to calculate the calibration coefficients $C_f(a_i)$, no additional error sources enter the simulation. The use of finite elements to determine calibration coefficients is commonplace and described in more detail elsewhere [34]. All calculations were carried out using the commercial code ABAQUS [35]. Using symmetry about the cut plane, half of the beam was modeled using 8-noded, quadratic shape function quadrilateral elements. On the cut plane, the mesh had 200 elements through the thickness of the beam, transitioning to a coarser mesh farther away. Incremental slit extension was simulated by removing the appropriate symmetry nodal displacement constraints on the slit plane in sequential analysis steps. To calculate the calibration coefficients, the element edges defining the exposed face of the slit were loaded with a non-uniform pressure distribution sequentially corresponding to $L_2(x)$ through $L_{16}(x)$. The remaining surfaces were taken as traction free. To calculate the strains for the two stress profiles for the simulation, the analysis was repeated for pressure distributions corresponding to Eqs. 19 and 20. Finally, strain for the gage centered on the symmetry plane was calculated by computing the relative displacement of the nodes corresponding to the center and end

of the strain gage and dividing by initial length between the nodes. Figure 3 shows the simulated strains for the two stress profiles.

3.3. Addition of Noise

The uncertainty analysis and order selection procedures were tested by simulating noise in the measured strain data. The simulated measured strains were randomized by adding an uncertainty vector

$$\{\varepsilon_r\} = \{\varepsilon\} + \{u_\varepsilon\}. \quad (21)$$

Each $u_{\varepsilon,i}$ was selected from zero-mean normal distribution using a random number generator. To examine different magnitudes of noise, the distribution was scaled to different standard deviations. The final stress results varied significantly between different sets of random strain added to the strain data. Therefore, to establish the average trends, each test case was repeated with 500 sets of randomized noise added to the strain data, each from the same underlying population of a given standard deviation and zero mean.

3.4. Stress, Error and Uncertainty Calculation

Each test case was examined over a large range of expansion orders, $n=1$ to 15. The A_j were calculated from Eq. 5, with $\{\varepsilon_r\}$ replacing $\{\varepsilon\}$ for the cases where noise in the strain data was simulated. The resulting stresses and fit strains were calculated using Eqs. 3 and 4. The stress uncertainty from random errors in the strain data were then evaluated using Eqs. 14 and 12. The model uncertainties were evaluated for series expansions $n=2$ to 14 using Eq. 16 with a 3-term model uncertainty with $a = n - 1$ and $b = n + 1$. For the noise-added test cases, the same set of noisy strain data was used for all 15 expansion orders before a new set was generated. Each depth-averaged error or uncertainty was then averaged over the 500 trials with different noise added to the data.

In order to best examine the numerical behavior of the calculations, the misfit strain, Eq. 14, is used for the strain uncertainty and no inherent experimental uncertainty value is considered. It will be shown that for the numerical examples considered, the misfit converges to the value of the added measurement noise.

The actual error e is evaluated by comparing the calculated residual stress distribution with the known stresses of Eqs. 19 or 20. The pointwise error at each x_i is just the difference between the calculated, $\sigma_{c,i}$, and known stresses, $\sigma_{k,i}$. A root-mean-square average value is calculated from the pointwise values:

$$\bar{e} = \sqrt{\frac{1}{m} \sum_{i=1}^m (\sigma_{c,i} - \sigma_{k,i})^2} \quad (22)$$

Because the stress profiles were normalized to give a peak magnitude of one, all of the stress errors and uncertainties can be considered as normalized to the maximum stress magnitude in the residual stress profile. Similar depth-averaged values were calculated for the measurement, model, and total uncertainties. The depth-averaged errors and uncertainties do not include the values at $x = 0$, which is considered an extrapolated value since the first data point is taken at the first cut depth.

4. Results and Discussion

The results from various test cases were examined to answer the most important questions. Does each error estimate accurately capture the actual error? Does selecting the expansion order based on the minimum estimated total uncertainty [19] give an optimal solution? The optimal expansion order is taken to be the one that minimizes the rms error between the calculated and actual stresses.

4.1. Polynomial no noise

The first case considered is the most straightforward but least realistic, the polynomial stress profile with no noise added to the strain data. Figure 4 shows the estimates of average uncertainty compared with the actual error over the full range of expansion orders. Until the expansion reaches four terms, covering the highest term in the polynomial, the actual errors are significant with a maximum average error of 28% of the peak stress. From four terms on, the actual error is zero to within machine precision. For $n < 4$, the measurement uncertainty estimated from uncertainties in the measured strains, s_{ϵ} , underestimates the actual errors by more than an order of magnitude. Underestimation was expected since the measurement uncertainty assumes that the model is correct, which it is not until n reaches 4. The model uncertainty does a very good job of estimating the actual error for $n=2$ and 3. The model uncertainty overestimates the error for $n=4$ because the estimate from Eq. 16 includes the $n=3$ solution. Selecting the order on minimum average total uncertainty would choose any of the expansions with 5 terms or more, which all have zero uncertainty or error.

The model uncertainty analysis provides an excellent estimate of not only the depth-averaged error but also the pointwise errors. Figure 5 shows the $n=2$ solution plotted with the pointwise total uncertainty estimate and the known stresses. For a normal distribution, the one standard deviation uncertainty would be expected to contain a given measurement with 68% probability. In Figure 5, the actual stress falls within the uncertainty bars at 34 of the 48 data points, or 69%. For the unplotsed $n=3$ solution, the actual stresses fall within the uncertainty bars at only 18% of the points, which is consistent with the underestimate of average total uncertainty shown in Figure 4. Both model and measurement uncertainty estimates capture the unequal distribution of errors, although the total uncertainty bars in Figure 5 are dominated by model uncertainty.

4.2. Gaussian no noise

The next test case is the Gaussian stress profile with no noise added to the strain data. In this case, the Legendre series expansion cannot exactly fit the known stresses for any fit order. Figure 6 shows that the actual error is significant for low order expansion and decreases to less than 1% for $n \geq 10$. The measurement uncertainty again underestimates the actual error, by about an order of magnitude. The model uncertainty does a good job of approximately capturing the actual error. Selecting the order on minimum average total uncertainty would choose the highest available order with estimated uncertainty, $n = 14$. Such a selection is expected for noiseless data and a non-polynomial stress distribution.

4.3. Polynomial with noise

The next test case is the polynomial stress with 500 sets of random noise added to the strain data. Figure 7 shows the results for noise with a standard deviation of 0.03, nearly 4% of the peak magnitude of the measured strain. The actual error drops precipitously at $n = 4$, the highest order term in the known stress, and then increases as higher order terms fit noise in the data. Up to $n = 3$, all of the uncertainty estimates are almost the same as Figure 4 since they are dominated by the inability for a lower order expansion to fit the higher order stress distribution. For $n \geq 4$, the measurement uncertainty essentially matches the actual error. The model uncertainty should ideally go to zero for $n \geq 5$, but it is equal to 68% of the measurement uncertainty for $n = 5$ decreasing to 54% at $n = 14$. Such behavior is an unavoidable consequence of the model uncertainty estimate. However, it will be shown that this phantom model error is not so large in the more general case of a non-polynomial stress distribution. In this example, because of the model uncertainty, the total uncertainty exceeds the actual error by 47% to 17% for $n = 5$ through 14, respectively. Selecting the order on minimum average total uncertainty would choose the $n = 5$ solution, just as in the polynomial test case with no noise.

A look at results for a typical single trial with noisy data shows what one might encounter with a typical real data set. Figure 8 shows the results for one of the 500 trials from Figure 7. There is much more variation in the actual error and the model and measurement uncertainties. The actual error increases non-smoothly with increasing order. The model uncertainty is the most irregular curve, which can be expected because of trying to capture a statistical average using only three samples. The measurement uncertainty curve is the smoothest, which is typical but may not always be the case. For this particular trial, selecting the order on minimum average total uncertainty still gives a good result but with the uncertainty overestimated.

4.4. Gaussian with Noise

The next test case is the most realistic, the non-polynomial stress distribution with noise added to the strain data. Again, results are averaged over 500 trials of random noise in order to reveal the underlying behavior of the uncertainty analysis. Figure 9 shows the results for noise with a standard deviation of 0.006, 1% of the peak magnitude of the measured strain. Up to about $n = 6$ all of the curves are very similar to the no noise case shown in Figure 6. After that the noise begins to have an effect and the errors tend to increase with increasing n . The actual error shows a broad minimum from $n = 6$ to 9. Selecting the order on minimum average total uncertainty would choose the $n = 7$ solution and give, somewhat fortuitously, an almost perfect estimate of total uncertainty. At high orders, the model error should ideally follow the trend of Figure 6 but, like the polynomial stress profile with noise, shows some influence from the measurement error. This phantom model error results in only a slight overestimation of the total error.

Less ideal results are possible. Figure 10 shows results of a test case with the Gaussian stress profile and the noise raised to 0.012, 2% of the peak strains. As it should, the increased noise results in increased errors at higher orders. Unfortunately the total uncertainty now shows two minima. The absolute minimum is at $n = 4$ where the actual error is 3.9 times its minimum value and the total

uncertainty underestimates the actual error by a factor of 3.3. The local minimum in total uncertainty at $n = 7$ would be a much better choice of expansion order with regards to finding the minimum actual error and estimating the uncertainty accurately. The inaccuracies arise because for this particular test case the model uncertainty is a poor estimate of the model error for $n = 3$ and 4. Using more terms in the model uncertainty estimate would provide a better estimate in this case but poorer estimates in some other cases.

4.5. Individual Strain Errors

The use of individual strain uncertainties, $u_{\epsilon,i}$ from Eq. 14, in the calculation of measurement uncertainty is somewhat unconventional but is more powerful. The other and more commonly used option is to populate the u_{ϵ} vector with a uniform value of the average strain error, \bar{u}_{ϵ} from Eq. 13 or from an *a priori* estimate of the uncertainty of the measurement equipment. The calculations for the noise-added test cases of Figure 7, Figure 9, and Figure 10 were repeated but using \bar{u}_{ϵ} . Using \bar{u}_{ϵ} gave higher measurement uncertainty for the expansion orders $n \geq 4$ for the polynomial and $n \geq 6$ for the Gaussian, by as much as 10% for the polynomial and 15% for the Gaussian. Since the calculations using $u_{\epsilon,i}$ match the actual errors virtually perfectly, this result does indicate that using \bar{u}_{ϵ} is less accurate. However, the difference is not very significant.

The next test case is chosen to illustrate when the difference is more significant. Since the issue involves the calculation of measurement error, the polynomial stress profile is considered so that the complicating issue of model error is minimized. The effect of a bad data point is exaggerated by reducing the magnitude of the 25th measured strain by 40%. No noise is added to the strains, so the measurement uncertainty all comes from the bad data point. Figure 11 shows the results. The oscillatory pattern in the actual error for $n \geq 4$ indicates that the bad data point has a different effect on odd and even ordered expansions. Once the expansion order reaches the highest

order term in the known stress polynomial, the measurement uncertainty calculated using $u_{\epsilon,i}$ matches the actual errors almost perfectly. The measurement uncertainty calculated using \bar{u}_{ϵ} exceeds the actual error by up to a factor of 2.5. The model uncertainty should be zero for $n \geq 4$ but instead tracks the magnitude of the actual errors rather well, albeit out of phase with the oscillations.

The issue of a bad data point is a practical one even though the test case was artificially constructed to best illustrate the issue. In slitting experiments, misleading data points can be encountered for deep slit depths, generally somewhere beyond $a/t = 0.95$. As the remaining ligament in the part becomes small, the measured strains are increasingly affected by the specimen weight rather than just the residual stresses. However, it is difficult to identify precisely at which depth the data should no longer be used. Using individual strain uncertainties make the results much less sensitive to the choice of the final data point used.

4.6. Effect of Covariant Terms

Figure 12 illustrates the importance of using the covariant terms in the uncertainty analysis. The $n = 10$ solution from a typical noisy trial from Figure 9 was examined. Figure 12a shows the solution compared to the known, Gaussian function plotted with uncertainty bars calculated correctly including covariances. The magnitudes of the uncertainties vary significantly with depth and correctly reflect the actual errors. The uncertainties are largest near the beginning of the cut, where the strain data had the smallest magnitudes and was more affected by noise. Figure 12b shows the uncertainty bars calculated with covariances set to zero. Although the uncertainties still vary somewhat with depth, they do not accurately reflect the actual errors. Repeating all the calculations of Figure 9 without including covariances, the estimated average measurement uncertainties exceed the actual errors by up to 30%.

4.7. Strain Fit Plateaus

An often used heuristic rule for selecting expansion order is a very useful supplement to the full uncertainty analysis but is less robust and often requires significant judgment. The order can be selected when the average strain misfit, \bar{u}_ϵ from Eq. 13, reaches a plateau as the least square fit converges [19]. Figure 13 shows \bar{u}_ϵ plotted versus n for the test cases. Values of \bar{u}_ϵ that were zero for the polynomial without added strain noise were set to 5×10^{-6} for plotting purposes. The figure also indicates the point for each curve corresponding to the minimum in average total uncertainty. Indeed, the minima generally occur in a plateau in the strain misfit. Because the model uncertainty for order n includes the $n - 1$ order solution, the minima tend to occur one point beyond the beginning of the plateau. For the suboptimal choice of $n = 4$ from Figure 10, Figure 13b shows that the final strain plateau is not reached until $n = 6$, indicating that examining the strain misfit would give some clue about choosing a higher order fit. However, the strain plateau is somewhat subtle; therefore, such a decision would not be obvious. The plateaus in Figure 13b all occur at the level of the noise added to the strain data, as should be expected.

4.8. Other Observations

Although not reported in detail because of space limitations, this study confirmed many observations and speculations reported previously. As is well known, the least squares fit makes the series expansion approach quite robust to random noise in the strain data [22,23]. Using a second strain gage at a well-chosen location can greatly reduce the sensitivity to errors [19,34,36]. The errors and uncertainties tend to decrease with an increase in the number of experimental data points m [37]. It was also found that sufficiently increasing the number of data points resulted in the optimal solution shifting to a higher n . These last two observations confirm the expectation that

taking more data points, i.e., using finer slit depth increments, can reduce the errors and increase the spatial resolution, within limits.

Since the optimum selection generally comes when the measurement uncertainty is the main contribution to the error, the procedure for optimizing strain gage placement based on minimizing the expected measurement uncertainty [34] is quite valid. However, a more accurate relative measure of expected global uncertainty can be achieved by replacing $[\text{DIAG}\{u_e^2\}]$ in Eq. 12 of this paper with the identity matrix and then root-mean-square averaging the individual $s_{e,i}$. Repeating the analysis for Figure 9 in [34] then shows that series based on Legendre polynomials, power series, or Fourier series result in approximately equal uncertainties rather than Legendre polynomials being vastly superior [38].

5. Experimental validation

Space limitations prevent the demonstration of this approach on experimental data. Fortunately, during its development the general approach has been applied to several slitting measurements and the results reported in the literature. Those results in the literature cover a fairly wide range of applications of slitting and demonstrate the versatility of the approach presented in this paper. Some papers include through-thickness measurements using only a single strain gage located opposite the cut [11,39], like the numerical results in this paper. For through-thickness measurements, some use two gages in order to improve the condition of the matrix inverse [11,36,39,40], and the results show clearly that the uncertainty is reduced. A few are near-surface stress measurements that only use strain gages on the top surface where the slit begins [15,24,41]. Such measurements are similar to hole drilling and show larger uncertainties than through-thickness measurements. One of the near-surface measurements included an intermediate step of finding the underlying inherent strains, and then was used to determine multiple stress components [15]. Both

the model error and strain error calculations of this paper were successfully applied to the inherent strain analysis. Finally, one result in the literature was for an unusual geometry that had relatively large uncertainties, a thin sheet with strain gages on the side [34]. Many of the results described in this paragraph show 90% uncertainty bars rather than one standard deviation, and the uncertainties were sometimes augmented by other error sources.

6. Conclusions

- The uncertainty analysis provides not only a good estimate of average uncertainty, but also a good estimation of the pointwise distribution of the uncertainties.
- Equation 16 provides a good estimate of the never before captured phenomenon of model uncertainty. However, the reliance on only a few fit orders to capture a statistical quantity reduces the robustness of the estimate.
- Minimizing the total uncertainty is an effective way to objectively select the expansion order. However, because of the statistical nature of the problem, the optimal solution will not always be selected.
- A heuristic approach of selecting the order based on a plateau in the strain misfit and then calculating the uncertainty based only on measurement uncertainty would tend to give reasonable results but require judgment. Including model uncertainty reduces the need for judgment and provides a better uncertainty estimate.
- Using the strain misfit helps prevent *a priori* estimates of inherent measurement uncertainty from underestimating the actual uncertainty.

Acknowledgments

Part of this work was performed at Los Alamos National Laboratory, operated by the University of California for the United States Department of Energy under contract W-7405-ENG-

36. The authors would like to thank C. Can Aydiner of Cal Tech, Peter Mercelis of the University of Leuven and Robert Schultz of Alcoa for thoughtful input on the uncertainty analysis. The authors would also like to thank Francois Hemez at Los Alamos for a valuable review of the manuscript.

7. Appendices

7.1. Variations on least squares fit

Sometimes, variations are made to the simple least squares fit in order to achieve a more optimal solution. In general, the analysis of Section 2.3 is still applicable with only minor modification. For example, when a weighted least squares fit is used [42], Eq. 4 becomes

$$[w][C]\{A\} = [w]\{\varepsilon_f\} \quad (23)$$

where $[w]$ is an $n \times n$ matrix usually with only diagonal entries. The least squares fit and $[B]$ are then given by the replacement for Eq. 5

$$\{A\} = \left[([C]^T [w][C])^{-1} [C]^T [w] \right] \{\varepsilon\} = [B]\{\varepsilon\}. \quad (24)$$

When such a weighted least-squares fit is used with a series expansion the model error procedure of Section 2.4 still applies and should be used.

Similarly, when Tikhonov regularization is used [43,44], Eq. 4 becomes something like

$$\left[[C]^T [C] + \beta [H]^T [H] \right] \{A\} = [C]^T \{\varepsilon_f\}. \quad (25)$$

The least squares fit and $[B]$ are then given by

$$\{A\} = \left[([C]^T [C] + \beta [H]^T [H])^{-1} [C]^T \right] \{\varepsilon\} = [B]\{\varepsilon\}. \quad (26)$$

The definition of strain uncertainty must be chosen with care in this case. Regularization is generally used not with a series expansion but with basis functions given by a uniform stress in each interval of material removal. In such a case, there can be as many unknowns as data points. For little

or no regularization, i.e., $\beta = 0$, the strain can be fit exactly given no misfit strains to use to estimate the strain uncertainty. A value corresponding to inherent uncertainty or noise in the data should be used. The model uncertainty estimate would also need to be changed because for Tikhonov regularization, usually β is varied instead of n .

7.2. Sample Script

The below script for the commercial matrix software MATLAB [45] shows an implementation of the stress calculation and uncertainty estimation described in this paper. All possible series expansion orders are calculated, some plots like the figures in the paper are made, and then the solution that minimizes the total average error is plotted and a table of results is reported to the screen. Interested users can contact the lead author for a sample of the data files used with the script.

```
% series.m
% anything after a "%" is a comment

clear

load epsilon.txt; % Text file with m strain data, 1 value each line
load a.txt; % Text file with m slit depths
load C.txt; % Text file with m x n C matrix
load P.txt; % Text file with m x n P matrix

m=length(epsilon);
N=size(C,2); % maximum value of n

for n=1:N; % loop over possible expansion orders
    Cn=C(:,1:n); % Take submatrix of C for fit order < N
    Pn=P(:,1:n); % Take submatrix of P for fit order < N
    A=pinv(Cn)*epsilon; % least squares fit using MATLAB functionality
    % could use A=(((Cn*Cn)^-1)*Cn)*epsilon to look like Eq. 5
    sigma(:,n)=Pn*A; % stresses per Eq. 3
    epsilon_fit=Cn*A; % fit strains per Eq. 4
    u_epsilon_bar(n)=norm(epsilon_fit-epsilon)/sqrt(m-n);
    % avg strain uncert. & misfit per Eq. 13 (just for plotting)
    u_epsilon=sqrt(m/(m-n))*(epsilon-epsilon_fit);
    % Individual strain uncertainties, Eq. 14
    B=pinv(Cn); % Eq. 5. Again, could replace with B=(((Cn*Cn)^-1)*Cn')
    V=B*diag(u_epsilon.^2)*B'; % Eq. 11
    s(:,n)=sqrt(diag(Pn*V*Pn')); % Eq. 8
end
```

```

for n=2:N-1;
    s_model(:,n)=std(sigma(:,n-1:n+1)'); % Model error per Eq. 16
    s_total(:,n)=sqrt(s(:,n).^2+s_model(:,n).^2);
        % Total error per Eq. 17
    s_total_bar(n)=norm(s_total(:,n))/sqrt(m); % Avg total error
end

% select minimum total error :
[minimum_s_total_bar,ntemp]=min(s_total_bar(2:N-1));
n_star=ntemp+1 % Because "min" starts at 2

% echo results to screen and make plots:
sprintf('%s', '    x    stress    +-')
fprintf('%8.3f %8.2f %8.3f\n',[a sigma(:,n_star) s_total(:,n_star)])

figure(1);
plot([2:N-1],s_total_bar(2:N-1),'-o')
title('uncertainty'),xlabel('n');

figure(2);
plot([1:N],u_epsilon_bar,'-o')
title('average strain misfit'),xlabel('n');

figure(3);
errorbar(a,sigma(:,n_star),s_total(:,n_star))
title(sprintf('n = %i',n_star)),xlabel('x'),ylabel('stress');

```

8. References

- [1] Lambert, J. W., 1954, "A Method of Deriving Residual Stress Equations," Proceedings of the Society for Experimental Stress Analysis, **12**(1), pp. 91-96.
- [2] Schajer, G. S., 1981, "Application of Finite Element Calculations to Residual Stress Measurements," Journal of Engineering Materials and Technology, **103**(2), pp. 157-163.
- [3] Popelar, C. H., Barber, T., and Groom, J., 1982, "A Method for Determining Residual-Stresses in Pipes," Journal of Pressure Vessel Technology, **104**(3), pp. 223-228.
- [4] Cheng, W., and Finnie, I., 1985, "A Method for Measurement of Axisymmetric Axial Residual Stresses in Circumferentially Welded Thin-Walled Cylinders," Journal of Engineering Materials and Technology, **107**(3), pp. 181-185.
- [5] Fett, T., 1987, "Bestimmung Von Eigenspannungen Mittels Bruchmechanischer Beziehungen (Determination of Residual Stresses by Use of Fracture Mechanical Relations)," Materialprüfung, **29**(4), pp. 92-94.
- [6] Petrucci, G., and Zuccarello, B., 1998, "A New Calculation Procedure for Non-Uniform Residual Stress Analysis by the Hole-Drilling Method," Journal of Strain Analysis for Engineering Design, **33**(1), pp. 27-37.
- [7] Garcia-Granada, A. A., Smith, D. J., and Pavier, M. J., 2000, "A New Procedure Based on Sachs' Boring for Measuring Non-Axisymmetric Residual Stresses," International Journal of Mechanical Sciences, **42**(6), pp. 1027-1047.
- [8] Ozdemir, A. T., and Edwards, L., 2004, "Through-Thickness Residual Stress Distribution after the Cold Expansion of Fastener Holes and Its Effect on Fracturing," Journal of Engineering Materials and Technology, **126**(1), pp. 129-135.

- [9] Oguri, T., Murata, K., and Sato, Y., 2003, "X-Ray Residual Stress Analysis of Cylindrically Curved Surfaces Estimation of Circumferential Distributions of Residual Stresses," *Journal of Strain Analysis for Engineering Design*, **38**(5), pp. 459-468.
- [10] Colpo, F., Dunkel, G., Humbert, L., and Botsis, J., 2005, "Residual Stress and Debonding Analysis Using a Fibre Bragg Grating in a Model Composite Specimen," *Proceedings of the Society of Photo-Optical Instrumentation Engineers (spie)*, **5758**, pp. 124-134.
- [11] Prime, M. B., and Hill, M. R., 2002, "Residual Stress, Stress Relief, and Inhomogeneity in Aluminum Plate," *Scripta Materialia*, **46**(1), pp. 77-82.
- [12] Cheng, W., 2000, "Measurement of the Axial Residual Stresses Using the Initial Strain Approach," *Journal of Engineering Materials and Technology*, **122**(1), pp. 135-140.
- [13] Qian, X. Q., Yao, Z. H., Cao, Y. P., and Lu, J., 2004, "An Inverse Approach for Constructing Residual Stress Using BEM " *Engineering Analysis With Boundary Elements*, **28**(3), pp. 205-211.
- [14] Beghini, M., and Bertini, L., 2004, "Residual Stress Measurement and Modeling by the Initial Strain Distribution Method: Part I - Theory," *Journal of Testing and Evaluation*, **32**(3), pp. 167-176.
- [15] Prime, M. B., and Hill, M. R., 2004, "Measurement of Fiber-Scale Residual Stress Variation in a Metal-Matrix Composite," *Journal of Composite Materials*, **38**(23), pp. 2079-2095.
- [16] Korsunsky, A. M., Regino, G., and Nowell, D., 2005, "Residual Stress Analysis of Welded Joints by the Variational Eigenstrain Approach," *Proceedings of the Society of Photo-Optical Instrumentation Engineers (spie)*, **5852**, pp. 487-493.
- [17] Smith, D. J., Farrahi, G. H., Zhu, W. X., and McMahan, C. A., 2001, "Obtaining Multiaxial Residual Stress Distributions from Limited Measurements," *Materials Science & Engineering A*, **A303**(1/2), pp. 281-291.
- [18] Schajer, G. S., and Altus, E., 1996, "Stress Calculation Error Analysis for Incremental Hole-Drilling Residual Stress Measurements," *Journal of Engineering Materials and Technology*, **118**(1), pp. 120-126.
- [19] Hill, M. R., and Lin, W. Y., 2002, "Residual Stress Measurement in a Ceramic-Metallic Graded Material," *Journal of Engineering Materials and Technology*, **124**(2), pp. 185-191.
- [20] Galybin, A. N., 2004, "A Method for Measurement of Stress Fluctuations in Elastic Plates." *Damage and Fracture Mechanics VIII: Computer Aided Assessment and Control. Eighth International Conference on Computer Aided Assessment and Control in Damage and Fracture Mechanics*, March 31-April 2, 2004, Crete, Greece 233-242.
- [21] Fontanari, V., Frenzo, F., Bortolamedi, T., and Scardi, P., 2005, "Comparison of the Hole-Drilling and X-Ray Diffraction Methods for Measuring the Residual Stresses in Shot-Peened Aluminium Alloys " *Journal of Strain Analysis for Engineering Design*, **42**(2), pp. 199-209.
- [22] Gremaud, M., Cheng, W., Finnie, I., and Prime, M. B., 1994, "The Compliance Method for Measurement of near Surface Residual Stresses-Analytical Background," *Journal of Engineering Materials and Technology*, **116**(4), pp. 550-555.
- [23] Prime, M. B., 1999, "Measuring Residual Stress and the Resulting Stress Intensity Factor in Compact Tension Specimens," *Fatigue & Fracture of Engineering Materials & Structures*, **22**(3), pp. 195-204.
- [24] Rankin, J. E., Hill, M. R., and Hackel, L. A., 2003, "The Effects of Process Variations on Residual Stress in Laser Peened 7049 T73 Aluminum Alloy," *Materials Science & Engineering A*, **A349**(1/2), pp. 279-291.
- [25] Vangi, D., 1997, "Residual Stress Evaluation by the Hole-Drilling Method with Off-Center Hole: An Extension of the Integral Method," *Journal of Engineering Materials and Technology*, **119**(1), pp. 79-85.

- [26] Beghini, M., Bertini, L., and Raffaelli, P., 1995, "An Account of Plasticity in the Hole-Drilling Method of Residual Stress Measurement," *Journal of Strain Analysis for Engineering Design*, **30**(3), pp. 227-233.
- [27] Beaney, E. M., and Procter, E., 1974, "A Critical Evaluation of the Centre Hole Technique for the Measurement of Residual Stresses," *Strain*, **10**(1), pp. 7-14.
- [28] Cheng, W., Finnie, I., Gremaud, M., and Prime, M. B., 1994, "Measurement of near-Surface Residual-Stresses Using Electric-Discharge Wire Machining," *Journal of Engineering Materials and Technology-Transactions of the ASME*, **116**(1), pp. 1-7.
- [29] Bevington, P. R., and Robinson, D. K., 1992, *Data Reduction and Error Analysis for the Physical Sciences*, McGraw-Hill, Inc, Boston, MA.
- [30] Schajer, G. S., 1988, "Measurement of Non-Uniform Residual-Stresses Using the Hole-Drilling Method .1. Stress Calculation Procedures," *Journal of Engineering Materials and Technology*, **110**(4), pp. 338-343.
- [31] Ersoy, N., and Vardar, O., 2000, "Measurement of Residual Stresses in Layered Composites by Compliance Method," *Journal of Composite Materials*, **34**(7), pp. 575-598.
- [32] Finnie, S., Cheng, W., Finnie, I., Drezet, J. M., and Gremaud, M., 2003, "The Computation and Measurement of Residual Stresses in Laser Deposited Layers," *Journal of Engineering Materials and Technology*, **125**(3), pp. 302-308.
- [33] Cheng, W., Finnie, I., and Ritchie, R. O., 2001, "Residual Stress Measurement on Pyrolytic Carbon-Coated Graphite Leaflets for Cardiac Valve Prostheses." *Proceedings of the SEM Annual Conference on Experimental and Applied Mechanics*, Portland, OR., 604-607.
- [34] Rankin, J. E., and Hill, M. R., 2003, "Measurement of Thickness-Average Residual Stress near the Edge of a Thin Laser Peened Strip," *Journal of Engineering Materials and Technology*, **125**(3), pp. 283-293.
- [35] ABAQUS 6.4, ABAQUS, inc., Pawtucket, RI, USA, 2003.
- [36] Aydiner, C. C., and Ustundag, E., 2004, "Residual Stresses in a Bulk Metallic Glass Cylinder Induced by Thermal Tempering," *Mechanics of Materials*, **37**(1), pp. 201-212.
- [37] Cheng, W., and Finnie, I., 1987, "A New Method for Measurement of Residual Axial Stresses Applied to a Multipass Butt-Welded Cylinder," *Journal of Engineering Materials and Technology*, **109**(4), pp. 337-342.
- [38] Rankin, J. E., personal communication.
- [39] Aydiner, C. C., Ustundag, E., Prime, M. B., and Peker, A., 2003, "Modeling and Measurement of Residual Stresses in a Bulk Metallic Glass Plate," *Journal of Non-Crystalline Solids*, **316**(1), pp. 82-95.
- [40] DeWald, A. T., Rankin, J. E., Hill, M. R., Lee, M. J., and Chen, H. L., 2004, "Assessment of Tensile Residual Stress Mitigation in Alloy 22 Welds Due to Laser Peening," *Journal of Engineering Materials and Technology*, **126**(4), pp. 465-473.
- [41] Prime, M. B., Prantil, V. C., Rangaswamy, P., and Garcia, F. P., 2000, "Residual Stress Measurement and Prediction in a Hardened Steel Ring," *Materials Science Forum*, **347-349**, pp. 223-228.
- [42] Cheng, W., In preparation.
- [43] Tjhung, T., and Li, K. Y., 2003, "Measurement of in-Plane Residual Stresses Varying with Depth by the Interferometric Strain/Slope Rosette and Incremental Hole-Drilling," *Journal of Engineering Materials and Technology*, **125**(2), pp. 153-162.
- [44] Schajer, G. S., and Prime, M. B., 2005, "Use of Inverse Solutions for Residual Stress Measurements," *Journal of Engineering Materials and Technology*, to appear.
- [45] MATLAB Release 14, The MathWorks, Natick, MA, USA, 2004.

Figure Captions

Figure 1. Some of the measurement methods that can use a series expansion solution for the stresses.

Figure 2. Through-thickness residual stress profiles used in beam simulations.

Figure 3. Simulated strain data for slitting experiment simulation and residual stress profiles from Figure 2.

Figure 4. Estimated root-mean-square (rms) average uncertainties compared to rms actual error for $n = 4$ polynomial stress profile with no added noise.

Figure 5. The $n = 2$ solution for the $n = 4$ polynomial stress profile plotted with one standard deviation estimates of total uncertainty. Even for the underfit solution, the uncertainty estimate is appropriate.

Figure 6. Estimated rms average uncertainties compared to rms actual error for Gaussian stress profile with no added noise.

Figure 7. Estimated rms average uncertainties compared to rms actual error for Polynomial stress profile and noise added to strain data. These values are averaged over 500 trials with different values of random noise.

Figure 8. Estimated rms average uncertainties compared to rms actual error for Polynomial stress profile with noise added to strain data. This is a typical result for a single set of random noise added to the measured strains.

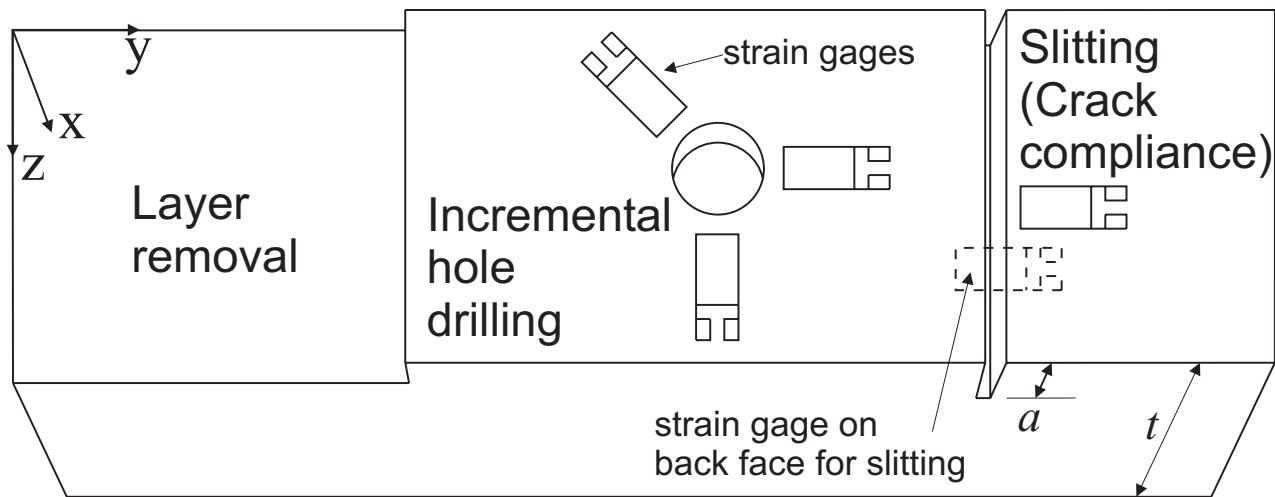
Figure 9. Estimated rms average uncertainties compared to rms actual error for Gaussian stress profile with noise with standard deviation of 0.006 added to strain data. These values are averaged over 500 trials with different values of random noise.

Figure 10. Estimated rms average uncertainties compared to rms actual error for Gaussian stress profile with noise with standard deviation of 0.012 added to strain data. These values are averaged over 500 trials with different values of random noise.

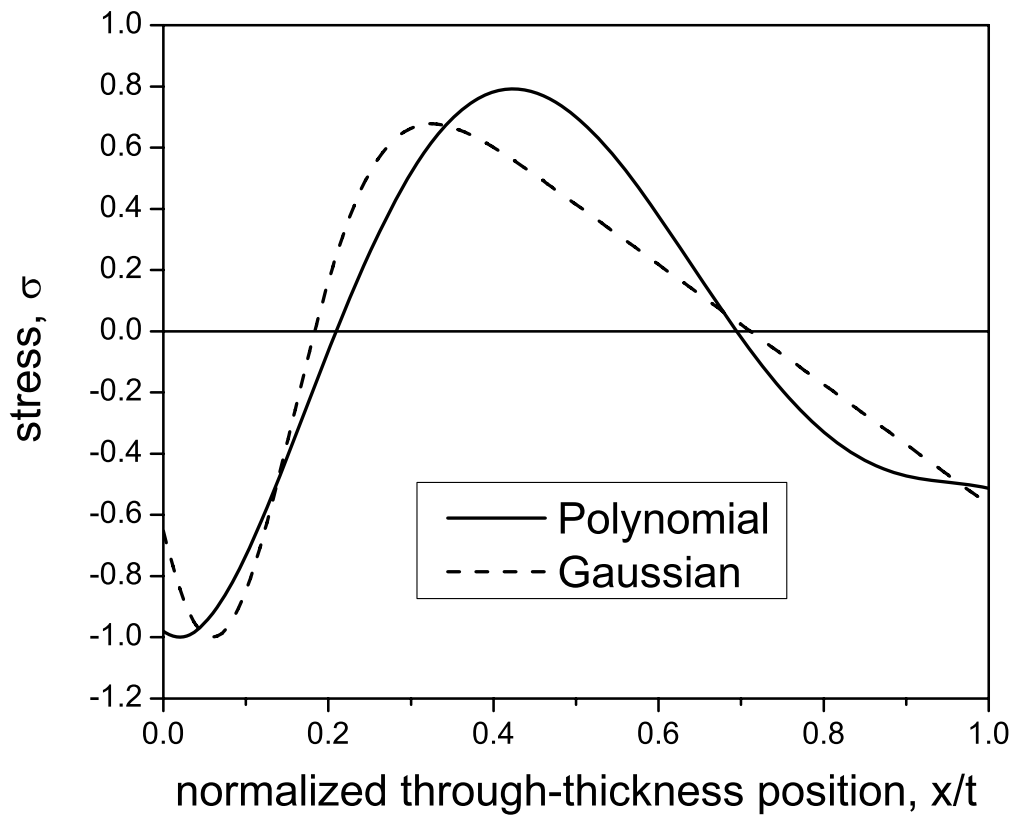
Figure 11. Estimated rms average uncertainties compared to rms actual error for polynomial stress profile with one bad data point and no added noise.

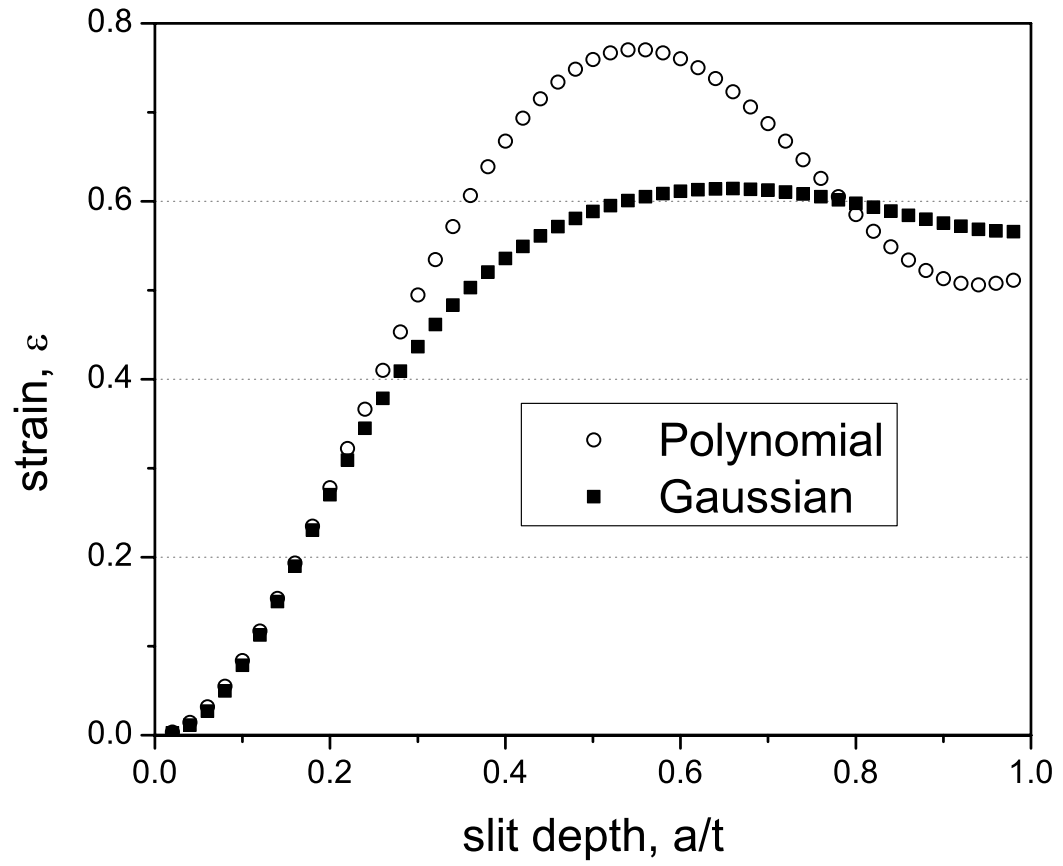
Figure 12. Solution from noisy data compared with actual, Gaussian stress distribution. Uncertainties calculated a) including covariances correctly reflect the actual errors and b) without covariances, the uncertainties are much less accurate.

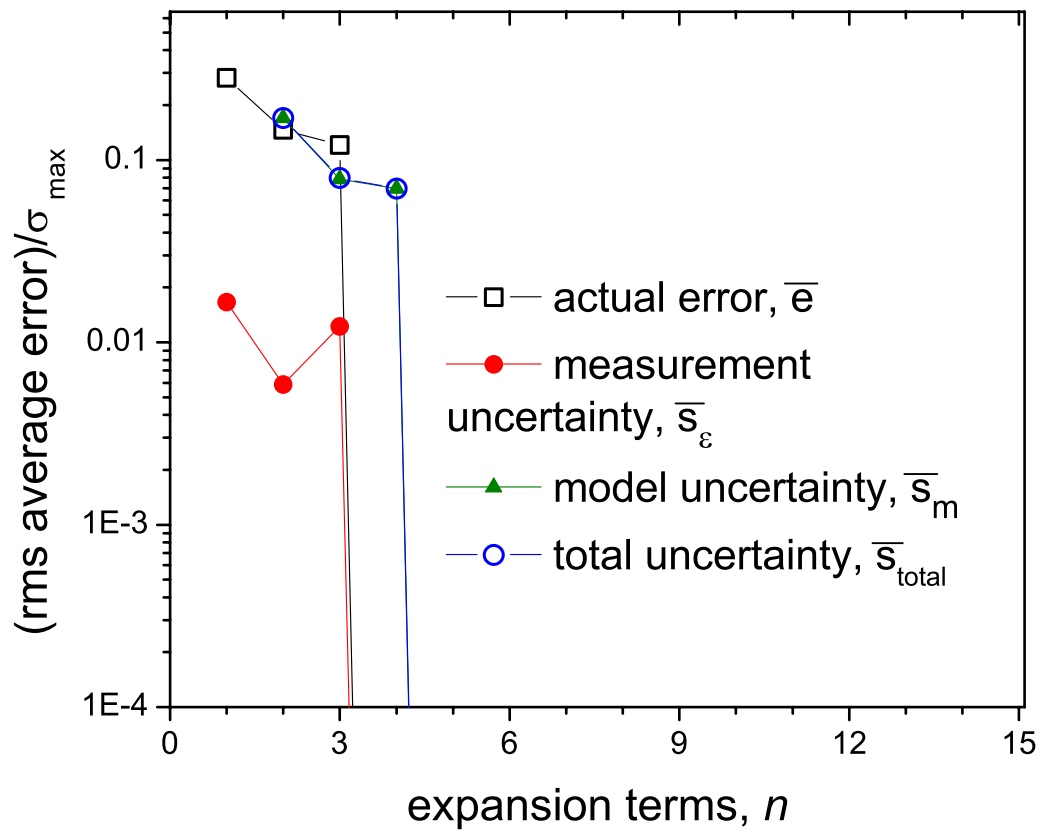
Figure 13. The rms average strain misfit as a function of expansion order for the 5 test cases. The points corresponding to minimum total uncertainty are indicated. a) full view; b) zoomed in on results for more realistic test cases with noise added to the strain.



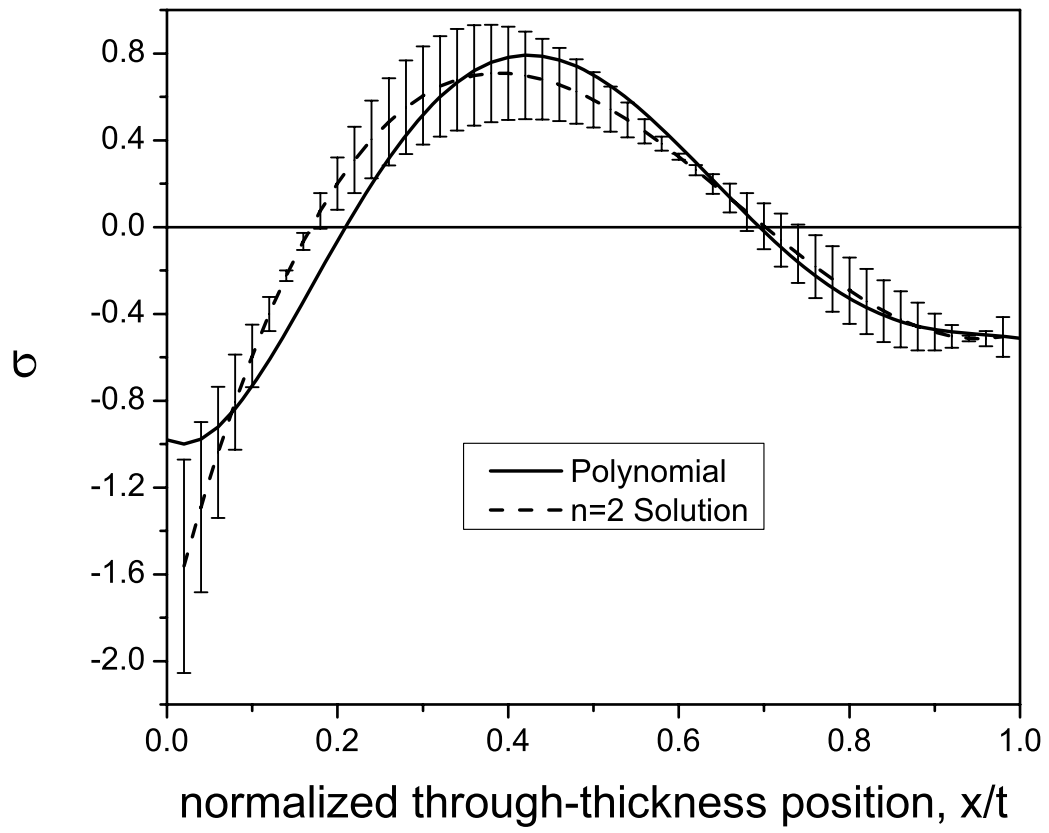
Prime and Hill, MATS-05-1056 Figure 1



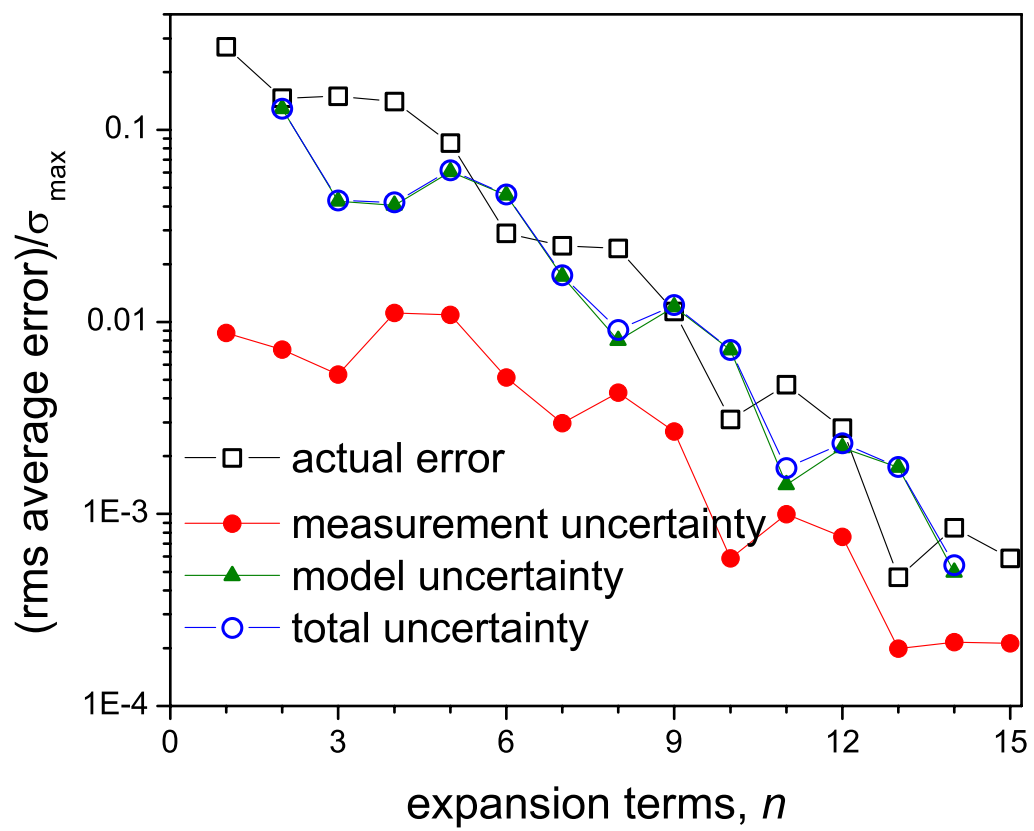


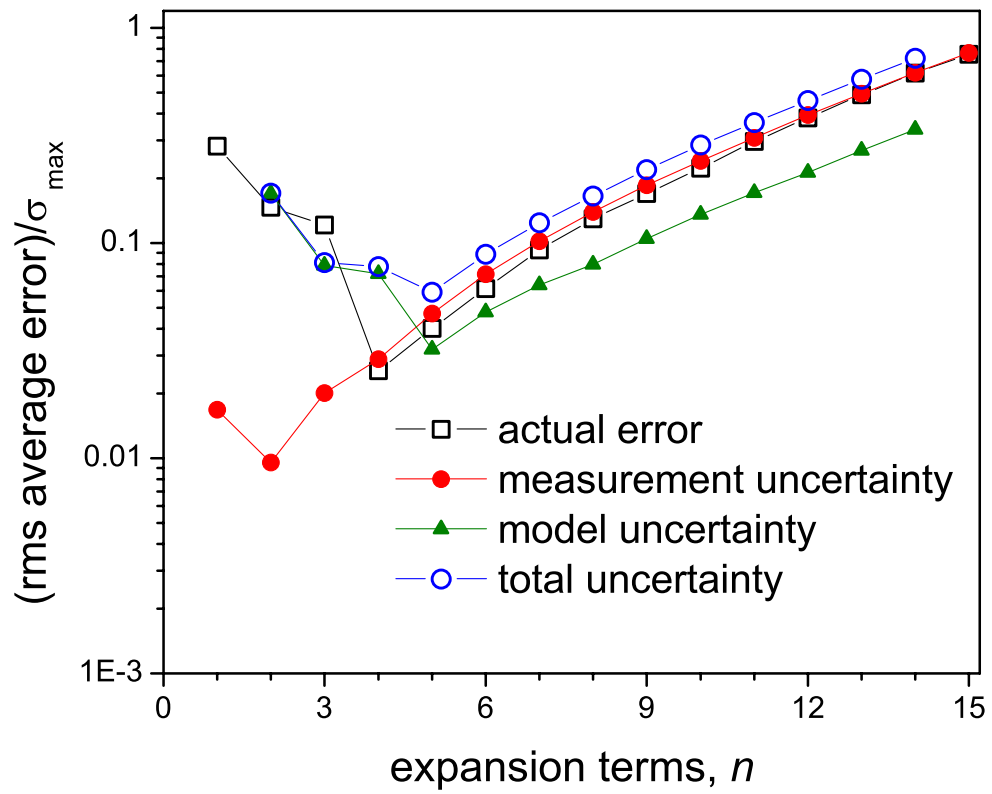


Prime and Hill, MATS-05-1056 Figure 4

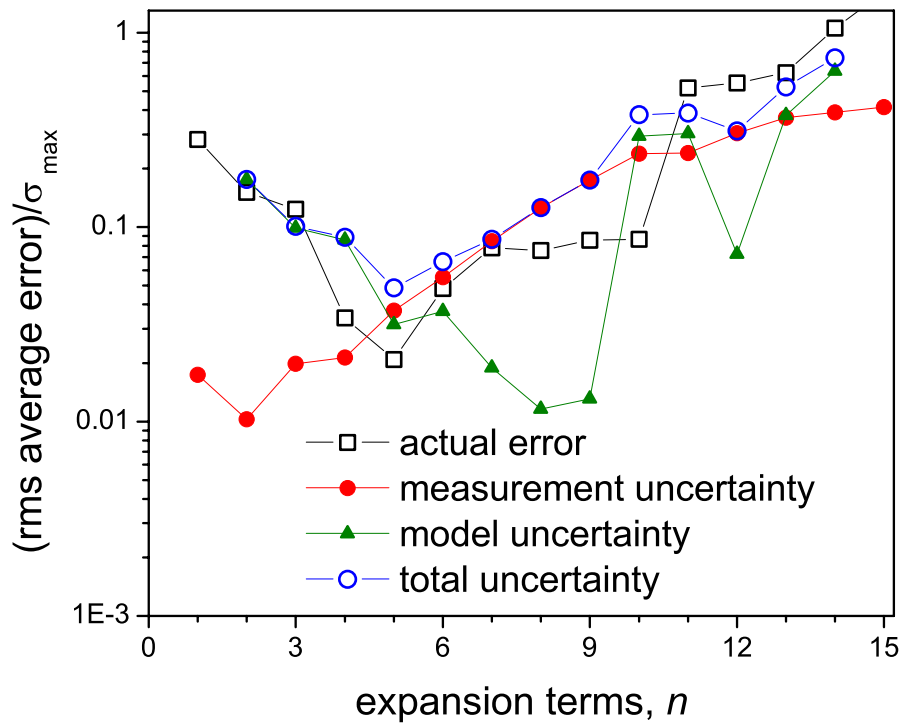


Prime and Hill, MATS-05-1056 Figure 5

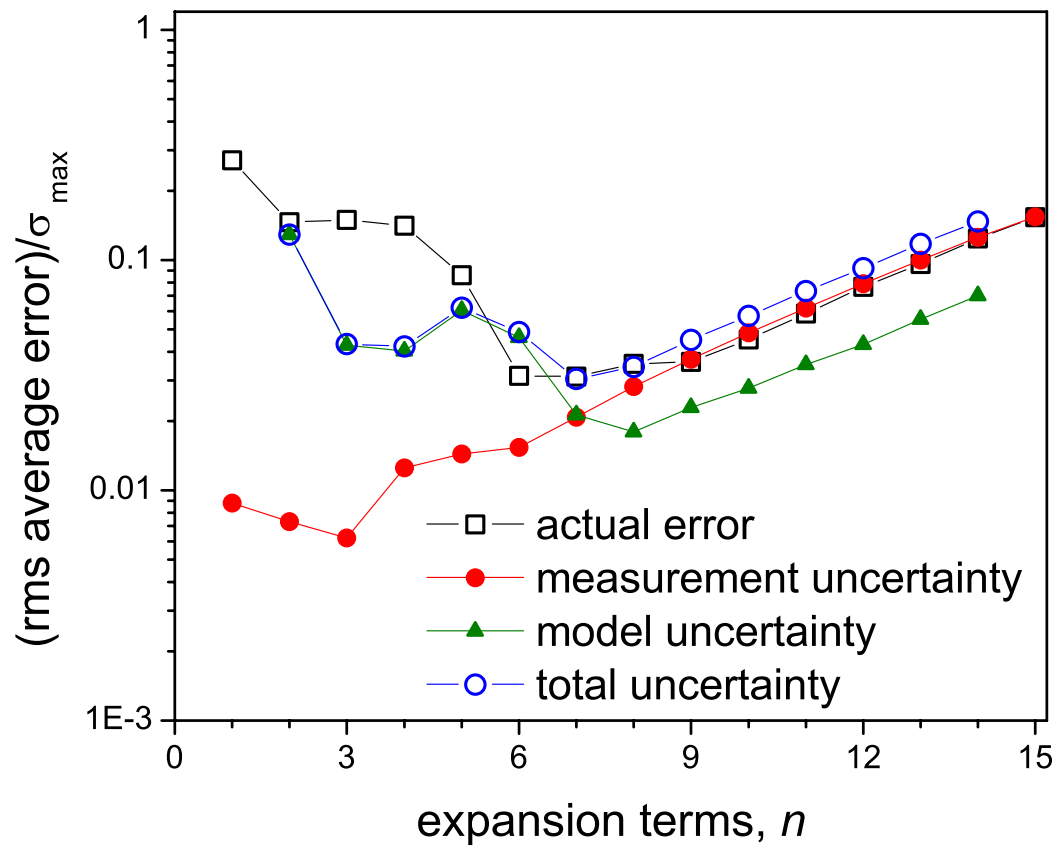




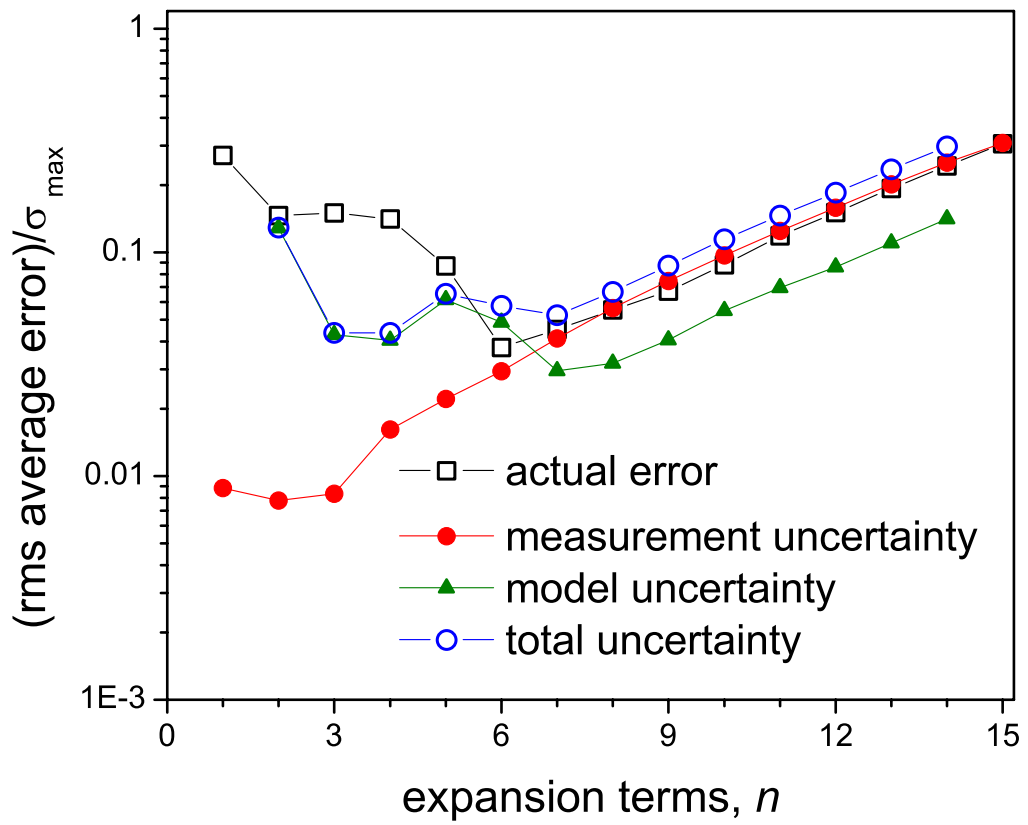
Prime and Hill, MATS-05-1056 Figure 7

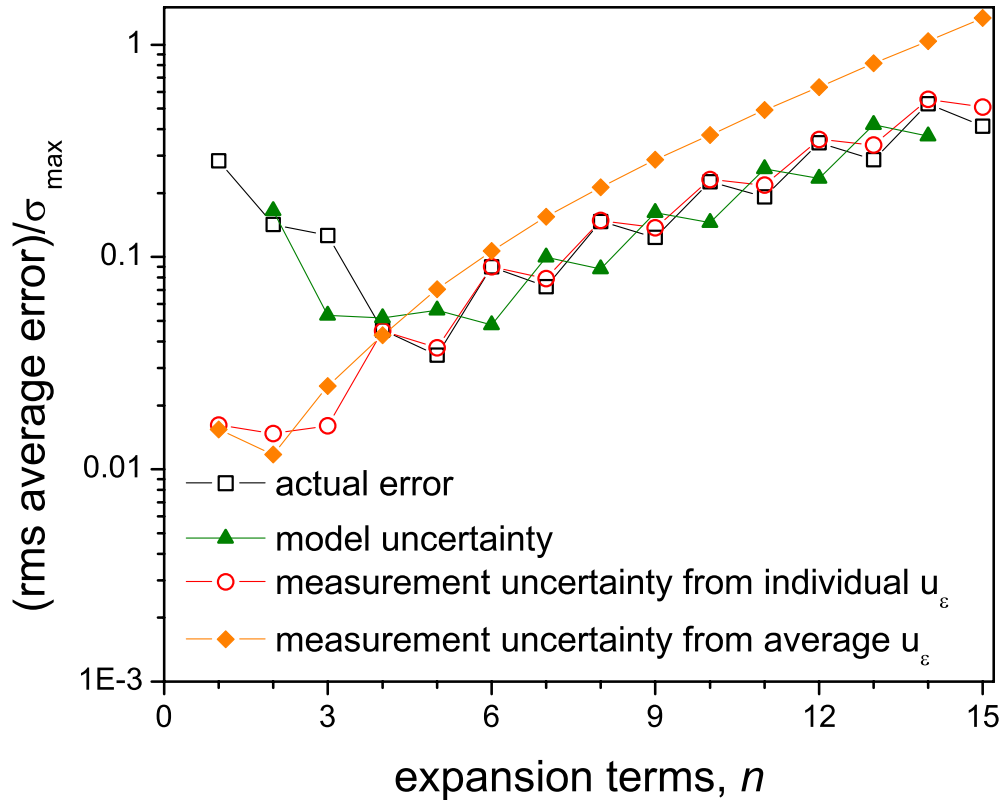


Prime and Hill, MATS-05-1056 Figure 8

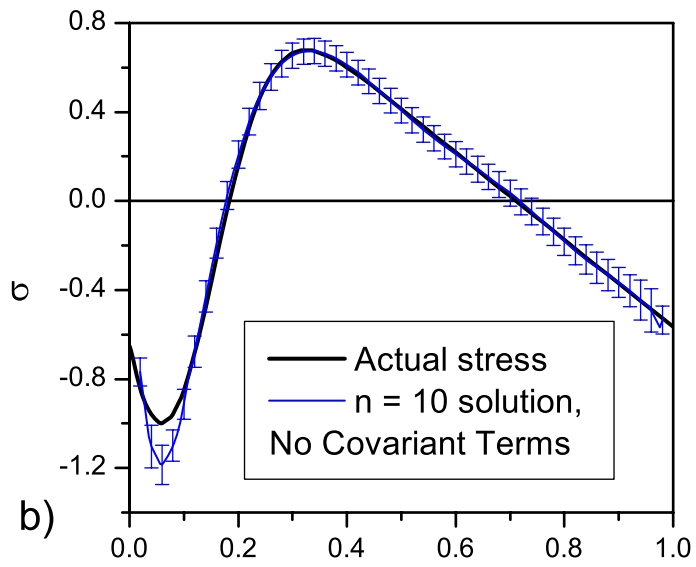
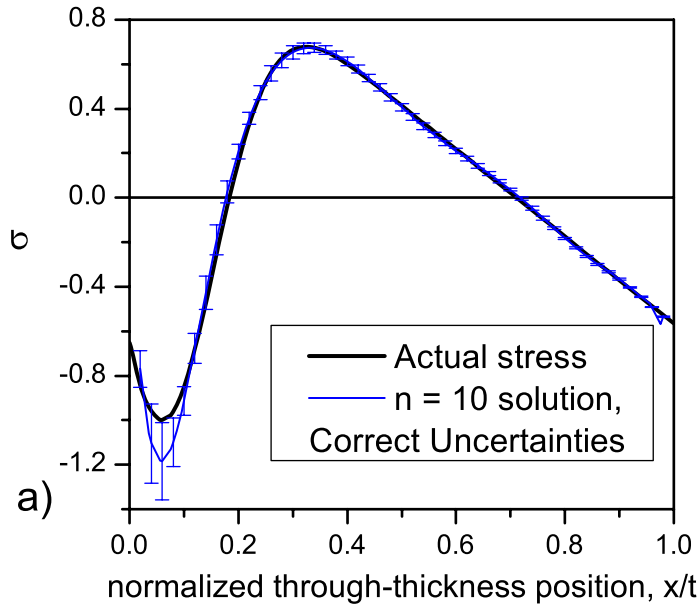


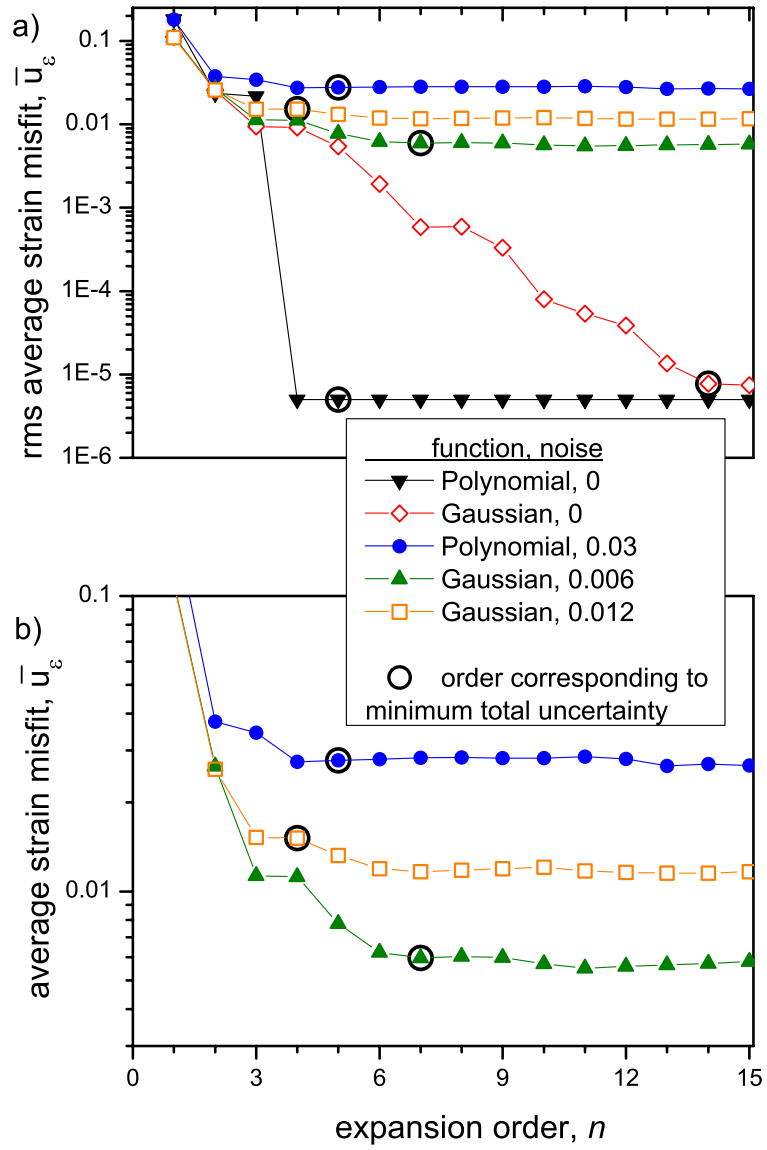
Prime and Hill, MATS-05-1056 Figure 9





Prime and Hill, MATS-05-1056 Figure 11





Prime and Hill, MATS-05-1056 Figure 13